Astron. Astrophys. 319, 18–32 (1997)

ASTRONOMY
AND
ASTROPHYSICS

X-ray sources $<$ 1 degree from Seyfert galaxies

H.-D. Radecke

Max-Planck-Institut für Astrophysik, D-85740 Garching, Germany

Received 25 March 1996 / Accepted 30 June 1996

Abstract. Archived PSPC observations of 26 Seyfert galaxies have been analyzed for bright X-ray sources out to the full extent of the field ($<$ about 50′). Of all Seyferts known this represents a sample 88% complete to $B_T = 10$ mag, 74% complete to 11 mag and 50% complete to 12 mag. Using the same reduction algorithm, 14 fields centered on stars at high galactic latitudes have been used as control fields. Excluding the two brightest Seyferts, a subset of 24 Seyferts with corrected apparent magnitude between $8.04 < B_T^{o,i} < 12.90$ mag show a minimum excess of 46 bright X-ray sources generally distributed between 10 and 25′ from the target galaxy. The significances of association of these sources with the Seyferts in the median brightness range are as high as 7.4 sigma.

Key words: galaxies: Seyfert – galaxies: spiral – X-rays: galaxies

1. Introduction

Studied extensively for the first time by Seyfert (1943) Seyfert galaxies have become a special laboratory for the analysis of active galaxies in the local part of the universe. Since they form the most common type of AGN at low redshifts they allow detailed studies of their morphological and dynamical characteristics over the whole observational window of astronomical instruments. A wide variety of morphological disturbances has been detected and analyzed within this class of objects, including extended HI emission (e.g. Mundell et al. 1995) and connections with nearby companion galaxies (e.g. Rubin and Ford 1968). Evidence is claimed by many authors (e.g. Barnes and Hernquist 1992 and references therein) for an important role of merger/tidal interactions in the fueling of the nuclear activity of Seyfert galaxies, and there are indications for an enhanced number of companions near Seyferts in comparison with "normal" disc galaxies: Studies by Petrosian (1982), Dahari (1985), and MacKenty (1989 and 1990) give an excess number of companions in the Seyfert environment, while Bushouse (1986) and Fuentes-Williams and Stocke (1988) could not find a significant excess. Very recently, Rafanelli et al. (1995) showed on the basis of two magnitude limited samples of 99 Seyfert 1 and 98 Seyfert 2 galaxies that there is a significant excess of companions around these objects with a lower limit percentage of 12% for both Seyfert types. Studying Seyfert galaxies on the basis of measurements on the Palomar Sky Survey, Laurikainen and Salo (1995) found that Seyferts have on average about twice the number of companions when compared with a control sample of comparison galaxies within a radius of 50 kpc, and three times more within 50 to 200 kpc.

While an excess number of galaxies within the close vicinity of a Seyfert does not in itself provide a proof for a decisive influence of tidal forces on the Seyfert activity (and even less is there a clear physical picture for the mechanisms linking Seyfert activity and interactions with companions) such an excess (if true) suggests a logical way to look for a mechanism which can ignite the active nucleus or generate disturbances within the galaxies.

Besides the optical work cited above, work on ROSAT X-ray data by Turner et al. (1993) showed, that also at high energies there is an indication of excess sources around Seyferts. The authors report results from a study of six Seyfert 2 galaxies using data in the soft X-ray (0.1 - 2.0 keV) band of the ROSAT PSPC. They found that the source density within a three arcmin radius around the target galaxies is on average a factor 8 higher than the mean density in the neighboring field. A physical association between the target sources and the companions is suggested. There is no firm identification of the companions found so far, and for one of the Seyferts (NGC 1365) the 5 companions found within the 3 arcmin circle coincide more or less well with the optical structure of the galaxy. It is not clear, however, whether these sources are situated within the Seyfert galaxy or are background objects.

The current study aims at an as complete as possible X-ray analysis of the environments of Seyferts down to a brightness of about 13 mag to determine the density of X-ray sources around the targets up to the full extent of the field of the ROSAT PSPC (i.e. $<$ about 50 arcmin). The comparison background source density is provided by the detailed log N/log S determination from the work of Hasinger et al. (1993). As for the completeness of the sample, the data available within the ROSAT archive as of October 1995 are 88% complete down to $B_T = 10$ mag, 74% complete to 11 mag, and 50% complete to 12 mag.

Send offprint requests to: H.-D. Radecke

2. Data analysis

2.1. The Seyfert sample

Table 1 shows the fields centered on Seyfert galaxies observed with the ROSAT PSPC which were available from the ROSAT archives as of October 1995. Only fields with an exposure greater than 6 ks were accepted. Three available fields were rejected: NGC 5506 with an exposure of only 4.5 ks, NGC 7590 because it is intermingeled with the close-by galaxy NGC 7582, and NGC 4388 because it is too close to the strong X-ray sources M 84 and M 86. The 26 remaining Seyferts listed in Table 1 are arranged in order of their apparent blue magnitude, corrected for galactic and internal absorption. This, the $B_T^{o,i}$ magnitude, is as given in the Revised Shapley Ames Catalog (Sandage and Tammann 1981). The realized exposure times are from those listed in the ROSAT archives.

2.2. The control sample

Hasinger et al. (1993) utilized 26 fields from the ROSAT medium sensitivity survey (RMSS) (in addition to the Lockman Hole) to determine the density of background extragalactic sources at high galactic latitudes. I have found 17 of these fields in the archives. Three of them (QSO 0000, QSO 1116, and QSO 1202) were rejected here on the grounds that they were extragalactic, Seyfert-like objects, somewhat fainter versions of the objects to be tested in this analysis. The remaining 14 are listed in Table 1. It is seen that the great majority of both control fields and Seyferts fall in the same range of galactic latitude $40^o \leq b^{II} \leq 80^o$.

Table 1. Fields analyzed

Object	Exposure (ks)	Gal.Lat. (deg)	Brightness (B, mag)	1/2 D_{25} (arcmin)	Seyfert	Type
NGC 5128	14.3	19	6.60	9.1	S2.0	S0pec
NGC 3031	49.8	41	7.01	12.9	S1.9	SbI-II
NGC 4258	7.2	69	8.04	9.1	S1.9	SbII
NGC 4945	14.2	13	8.30	10.0	S2.0	Sc
NGC 4594	10.6	51	8.40	4.5	S1.9	Sa/Sb
NGC 1068	9.3	-52	9.03	3.6	S2.0	SbII
NGC 1365	8.8	-55	9.45	4.9	S1.8	SBbI
NGC 1097	9.6	-65	9.75	4.7	S1.0	SBd-cI-II
NGC 1566	17.8	-44	9.79	3.8	S1.5	ScI
NGC 5005	9.0	79	9.81	2.7	S2.0	SbII
NGC 4579	9.4	74	10.01	2.7	S1.0	SabII
NGC 5033	8.0	80	10.11	5.2	S1.9	Sb-cI-II
NGC 4395	17.1	82	10.35	6.4	S1.8	SdIII-IV
NGC 4151	38.1	75	10.53	2.9	S1.5	Sab
NGC 4051	49.5	70	10.56	2.5	S1.5	SbcII
NGC 7213	8.9	-53	10.72	0.9	S1.0	Sa
NGC 3227	19.6	55	10.92	2.8	S1.5	SbIII
NGC 7314	19.3	-60	11.11	2.3	S1.9	ScIII
NGC 3998	62.9	60	11.50	1.5	S1.0	S0
NGC 4639	6.6	80	11.57	1.4	S1.8	SBbII
NGC 2992	18.6	29	11.61	2.0	S1.9	Sapec
NGC 2639	9.0	38	11.90	1.0	S1.9	Sa
NGC 4235	19.4	69	12.00	2.1	S1.0	Sa
NGC 3516	13.1	42	12.34	1.1	S1.2	SB0
NGC 5273	9.4	76	12.42	1.5	S1.9	S0/a
NGC 5548	19.3	71	12.90	1.0	S1.2	Sa
Pavo	25.1	-77				
LHS 2924	18.3	68				
ON 231	10.4	83				
HR 8905	26.3	-35				
CY Uma	9.4	59				
Uma	9.2	56				
Alpha Bootis	17.1	69				
F 1557	21.3	-42				
HR 857	10.7	-58				
GRB 190406	19.5	-40				
4 Dra	15.4	48				
EF Eri	15.8	-58				
EX Hya	15.6	34				
VW Hyi	8.1	-38				

Comments: B = Apparent blue magnitude, corrected for galactic and internal absorption. D_{25} = Apparent major isophotal diameter at surface brightness level 25.0 B-m/ss.

2.3. The source detection algorithm

In order to be able to check the derived control field densities against previous derivations the same source detection algorithm was used as described in detail in Hasinger et al. (1993). First of all the hard band (H) was utilized, i.e. the energy range between 0.5 and 2.0 keV. The hard band image of each of the target fields has a pixel size of $8''$. The source detection algorithm first scans each image to detect a significant excess over the background by guiding a detection cell of dimension $48'' \times 48''$ with a step size of one third of the cell across the image. A two-step detection method is then determining the relevant parameters of the sources. In a first step the background of the immediate surrounding of the detection cell is used while the second step employs a global background map to locate the X-ray excess. Those pixels in which sources have been found in the earlier step are removed from the image before this map is generated by smoothing the PSPC image with a bi-cubic spline function.

The source positions determined by this procedure are then merged. If different sources are found within the merging radius of $32''$ only the one of them with the highest likelihood is preserved. The optimal source positions are then determined by a maximum likelihood method described by Cruddace et al. (1988). Poisson statistics determines the probability for the source counts of being due to pure background fluctuation after comparing with the expectation value from the background map. A detection threshold of a likelihood of 10 (or about 4 sigma) was set for the current analysis, in accordance with the study of Hasinger et al. (1993). For a more detailed description of the procedures used here and further background see Hasinger et al. (1992), Hasinger et al. (1993), Voges (1992), and Briel et al. (1988).

The count rate was converted to flux by assuming a power law of index 1. The correction for galactic HI absorption has been carried out for each field using the data given in Dickey and Lockman (1990). The counts to flux conversion factor for the hard band is given by

$$F_x(10^{-13}\ erg\ cm^{-2}\ sec^{-1}) = 0.114\ C \quad (C = counts\ ks^{-1}).$$

As can be seen from Fig. 1a, the derived log N/log S curve fits very well the Hasinger et al. determination of background density (reproduced as the dashed line). The Hasinger et al. log N/log S relation was subsequently well confirmed by Vikhlinin et al. (1995), despite using a slightly different counts to flux conversion factor of 0.123 C.

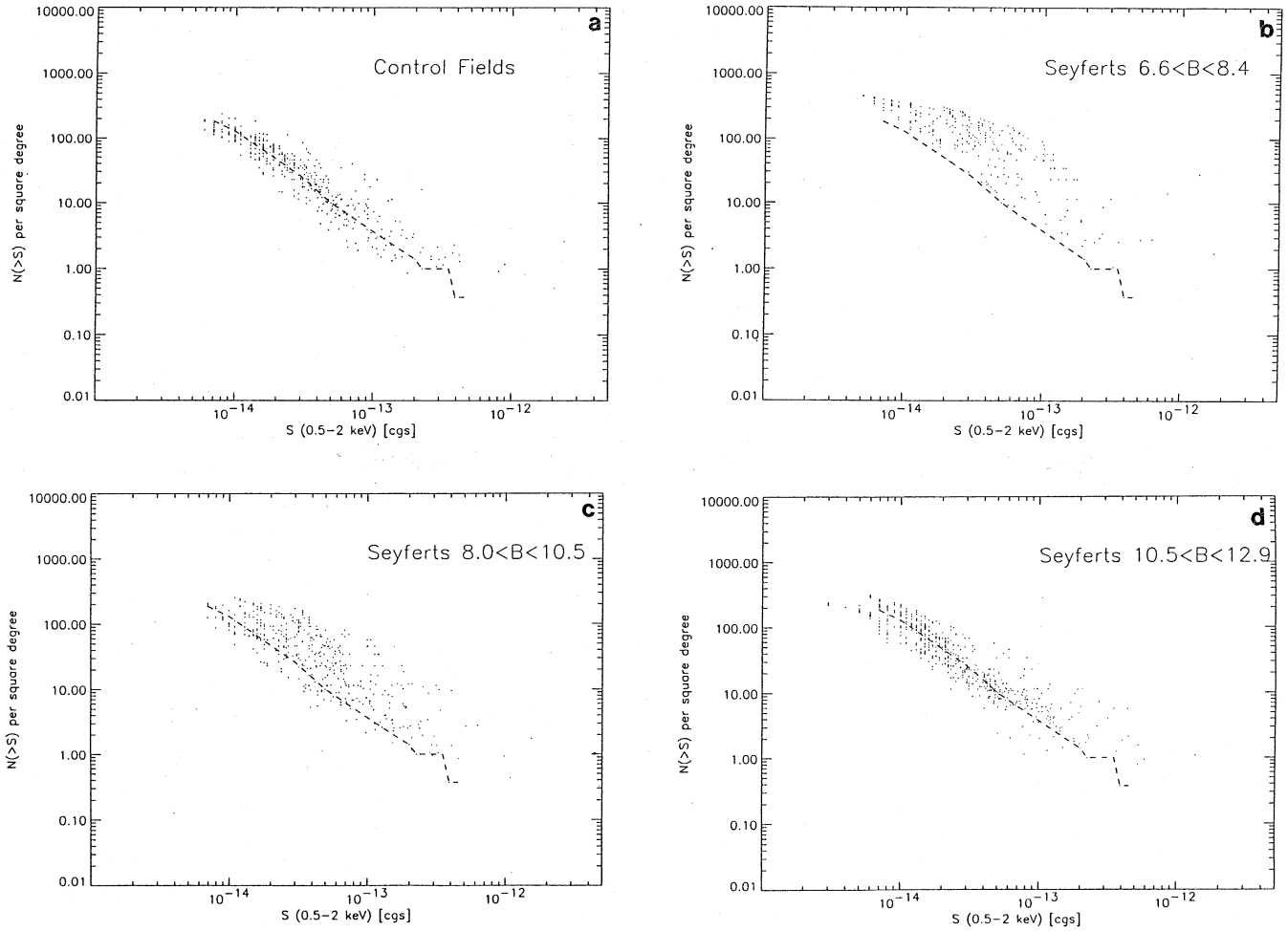

Fig. 1a–d. Log N/log S diagrams of the 4 samples analyzed. The dashed line in each panel represents the log N/log S curve determined by Hasinger et al. (1993). **a** Log N/log S curve of the 14 control fields. Note that the Hasinger et al. line is reproduced very well by the method used in this paper. **b** Log N/log S curve of the five brightest Seyfert galaxies analyzed. **c** Log n/log S curve of the 12 Seyferts of intermediate brightness. **d** Log N/log S curve of the 12 faintest Seyfert galaxies analyzed.

2.4. The determination of log N/Log S

The identical detection algorithm which was used to list sources in the control fields was also used to list the sources in the Seyfert fields. The thus detected sources for both Seyferts and control fields for $C > 5$ are given in the table in Appendix A.

The density of sources in each field was calculated in the following manner: The distance to either the first or the second brightest source, whichever was larger, was used to determine the number per square degree of sources as bright or brighter than the second brightest source. (The reason this was not calculated for the first brightest is because this would represent an uncertainty of ± 1 source, or the entire computed density.) Within the area encompassed at the radius r of the third brightest source all sources as bright or brighter were then used to compute N (per square degree) > S. The same procedure was repeated for the fourth brightest source, etc. until the area inside 10 arcmin was reached where N > S was computed using that fixed area (for all sources with r<10 arcmin.)

The purpose of performing the calculation in this way was to calculate from the actually observed brightest sources their exact areal densities.

Identically the same procedure was used on the 14 control fields. The result is shown in the 4 panels of Fig. 1.

3. Results

3.1. The log N/log S curves

Fig. 1 gives the log N/log S curves determined according to the procedure described in Section 2. Comparison of the four panels shows that the average density per square degree of X-ray sources is clearly greater in the Seyfert fields than in the fields not containing active extragalactic objects. There are several points to be noted about the four samples in Fig. 1:

1) The source detection and averaging procedure yields very closely the same average log N/log S curve found for the extragalactic X-ray background by Hasinger et al. (1993). The dashed

line in each panel in Fig. 1 shows that previously determined background as a reference level.

2) The results from the five brightest Seyferts are shown in Fig. 1b. Here the counts are dominated by the three nearest Seyferts, NGC 5128 (Cen A), NGC 4945, and NGC 3031 (M81). Relatively few background sources are present and the majority of sources clearly belong to the galaxies. Taking the average distance to the galaxies in this group as 3.3 Mpc, a source of luminosity $L_x = 2\times10^{38}\ erg\ s^{-1}$ would give a hard band flux of $S = 1.2\times10^{-13}\ erg\ cm^{-2}\ s^{-1}$. This is the point in Fig. 1b where the number of excess sources over the background diminishes sharply. Since $L_x = 2\times10^{38}\ erg\ s^{-1}$ is the limit of typical bright X-ray sources in our own galaxy, the bulk of the sources in Fig. 1b should be normal X-ray binaries, supernova remnants etc. But there are a few excess sources brighter than this which have no present identification with known kinds of X-ray sources. 8 such luminous objects in M 81 have been discussed by Fabbiano (1988) and 8 in M 51 by Marston et al. (1995).

3) The 12 Seyferts between NGC 4258 ($B_T^{o,i} = 8.04$ mag) and NGC 4151 ($B_T^{o,i} = 10.53$ mag) in Fig. 1c average 2.5 mag fainter than the dominant Cen A and M 81 in Fig. 1b. Therefore the dominant population of normal sources is moved by a factor of about 10 fainter in Fig. 1c and is no longer contributing significantly to the excess sources observed. The most conspicuous excess is now at luminosities $4\times10^{38} \le L_x \le 4\times10^{39}\ erg\ s^{-1}$. These represent a large number of sources of unknown type, more than an order of magnitude more luminous than the brightest galactic sources known. We will also see that they reside almost entirely outside the optical confines of the target galaxy.

4) The 12 faintest Seyferts between NGC 4051 ($B_T^{o,i} = 10.56$ mag) and NGC 5548 ($B_T^{o,i} = 12.90$ mag) in Fig. 1d average another 2.5 magnitudes fainter than the Seyferts in Fig. 1c. If this faintest Seyfert group is at 2.5 mag greater a distance modulus then the L_x of these sources reaches $6\times10^{40}\ erg\ s^{-1}$. This represents sources 300 times brighter than the galactic X-ray source upper limit.

(It is of course always implicitly assumed in these remarks that the detected sources are at the same redshift distance as the target galaxies.)

Although Figs. 1a-d are useful in demonstrating the general nature of the excess sources around this sample of Seyferts, the following analysis will examine which kinds of sources have the highest significances of association. One of the results which will emerge is that the highest luminosity sources are the most widely separated from the active galaxy.

3.2. Excess of X-ray sources around Seyferts from the raw counts

Appendix A lists the sources with C>5 ($F_x > 0.57$) which were measured around the Seyfert galaxies and control fields. Considering only sources of C>5 effectively removes the exposure effect on numbers of sources detected because even moderate exposure times detect to this level out to $\approx 40'$. This can be checked by plotting sources detected vs. exposure time where it is verified that there is no obvious relation.

Proceeding along the line of Hasinger et al. the inner 5 arcmin of a field have been excluded from the analysis if the target object is very bright. Within the sample of control fields this concerns only EX Hya. For the Seyfert sample, NGC 3516, NGC 5548, and NGC 7213 have been analyzed in this way.

If we count all sources with C>5 in the 26 Seyfert fields (322) and the 14 control fields (126) we obtain 12.38 sources per Seyfert and 9.0 sources per control field; this gives a significance for being a true excess of 4.1 sigma. If we accept only Seyferts and control fields with exposures between 8 and 30 ks we compute again a 4.1 sigma result. But if we count only the 14 brightest Seyfert fields with $6.6 < B_T^{o,i} < 10.5$ mag we obtain 13.57 sources per Seyfert and a 4.5 sigma result.

Two of the Seyfert target galaxies (NGC 2992 and NGC 3227) are known bright optical doubles. But in general there are no known counterparts to the detected X-ray sources.

In the following section we examine that part of the source intensity - off-axis diagram where field contamination is least, the Seyfert associated sources have the highest contrast and the significance of the association is highest.

3.3. Which sources are associated with the Seyferts?

In order to determine to what degree the sources are associated with the Seyferts and where they are located it is necessary to plot all sources in the galaxy fields as a function of count rate (C) and off-axis radius (r) and then compare to the same plots for the control fields. It is clear that background sources are encountered increasingly at larger r (area increasing) and smaller C (number of background sources increasing with faintness). Therefore sources associated with the galaxies were least contaminated by the background at small r and large C. Empirically the excess of Seyfert sources becomes noticeable at about r<25 arcmin. Fig. 2 shows the C,r-relation for all 26 Seyferts (a) and all control fields (b). For clarity of the presentation, a cut was made at a counts rate of 150 counts per kilosecond. 9 sources are omitted in this way from the Seyfert sample and 3 from the control fields. Fig. 3 gives the source densities for the 12 Seyfert fields within the brightness range $8.0 \le B_T^{o,i} \le 10.5$ mag compared to the densities for the 12 control fields defined below. Two cuts have been applied to the flux values: $10^{-13}\ erg\ cm^{-2}\ sec^{-1}$ (panel a) and $0.6\times10^{-13}\ erg\ cm^{-2}\ sec^{-1}$ (panel b).

For the convenience of doing statistics the source lists were divided in 3 groups:

1) 12 control fields. These are the fields listed in Table 1 with EX Hya omitted because it contains a strong X-ray cluster and a strong X-ray Parkes radio source. VW Hyi is omitted because it is the control field with the least exposure.

2) The 12 brightest Seyfert fields except Centaurus A (NGC 5128) and M 81 (NGC 3031) with $8.0 \le B_T^{o,i} \le 10.5$ mag.

3) The 12 faintest Seyfert fields with $10.5 \le B_T^{o,i} \le 12.9$ mag.

In each of these 3 groups totals were then made of the number of sources with $C > 10$, $r < 25$ arcmin. The 12 control fields contained 12 such sources. The Seyfert fields had a total of 52. Subtracting from this number twice the source count

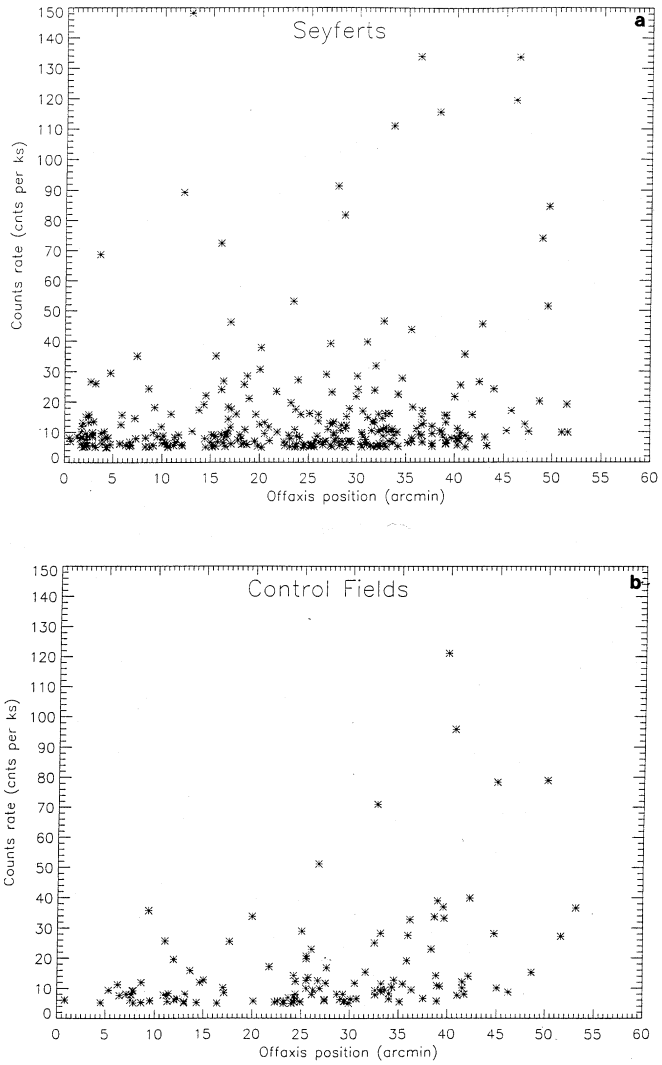

Fig. 2a and b. Count rates (counts per kiloseconds) vs. offaxis radius (arcmin) for all detected sources below 150 counts per kiloseconds. **a** all Seyfert fields, **b** all control fields.

found in the 12 control fields (i.e. 24) yields an excess of 28 sources for the 24 Seyfert fields or an average of 14 for each of the Seyfert samples of 12 fields. Taking the standard deviation of the control field number to be its square root gives a significance of $14/\sqrt{12} = 4.1$ sigma for $r < 25$ arcmin, $C > 10$. But, of course, for sources of intensity $5 < C < 10$ there are also conspicuous Seyfert excesses in the range $10' < r < 20'$ - a total of 18 objects (For this C-range, beyond r=20 arcmin, the background contamination begins to become larger. The cut is made on the $r < 10$ arcmin side in order to stay well away from the body of the Seyfert galaxies and any sources that might be contained within.) Therefore an average of 18 Seyfert sources and 8 control field sources are added. This yields a significance of: $23/\sqrt{20} = 5.1$ sigma for $r < 25'$, $C > 10$ plus $10' < r < 20'$, $5 < C < 10$.

This is for the 24 Seyfert galaxies with $8.04 \leq B_T^{o,i} \leq 12.90$ mag. If we do the same calculation for the 12 intermediate brightness Seyferts ($8.04 \leq B_T^{o,i} \leq 10.5$ mag) the following

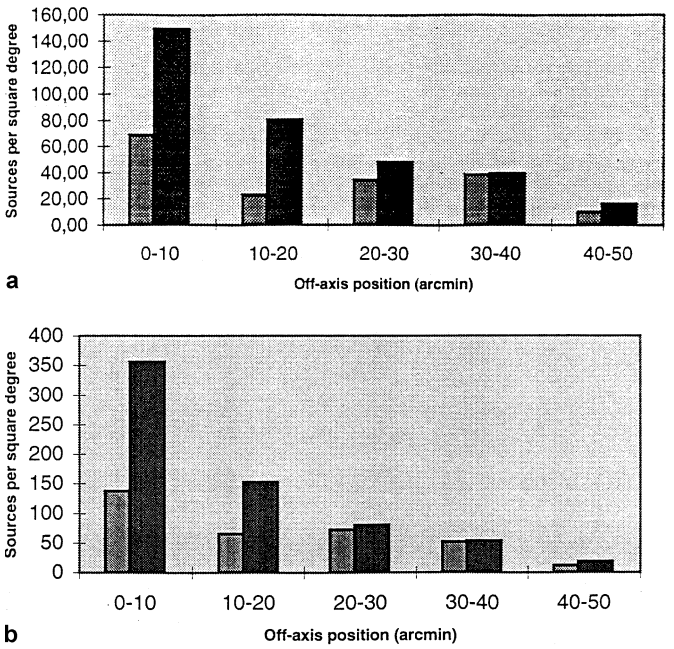

Fig. 3a and b. Histogram representation of the source density per 10 degree annulus for the brightest Seyfert sample with $8.0 \leq B_T^{o,i} \leq 10.5$ mag (black) and the control sample (gray). **a** includes all sources with a flux greater than 10^{-13} $erg\ cm^{-2}\ sec^{-1}$, **b** shows all sources above 0.6×10^{-13} $erg\ cm^{-2}\ sec^{-1}$.

significances are arrived at: $17/\sqrt{12} = 4.9$ sigma for $r < 25'$, $C > 10$ and $33/\sqrt{20} = 7.4$ sigma for $r < 25'$, $C > 10$ plus $10' < r < 20'$, $5 < C < 10$. It is reasonable and instructive in this case to add up these excesses because they cover the least contaminated and therefore most reliable area of the r,C-plane.

Therefore we see that the whole sample of 24 Seyferts has a significant association of bright X-ray sources at $r > 10'$ but that the 12 Seyferts in the sample of intermediate brightness have particularly significant associations. It is reasonable to suppose that as the Seyferts become more distant it is more difficult to detect their excess sources, which are fainter, against a constant background contamination.

The preceding counts were only of the excess of Seyfert sources in the region of the r,C-plane which is least contaminated by background objects. No attempt has been made here to estimate the number of Seyfert sources with $5 < C < 10$, at other radii or of sources fainter than $C = 5$. Nevertheless it is interesting to note that the number of excess sources within the analyzed area of the r,C-plane, i.e. 46, gives an approximate excess of 2 strong X-ray sources per Seyfert field. That would be sufficient for nearly every Seyfert galaxy to have a pair of strong X-ray sources within a radius of $25'$.

4. Discussion

The analysis presented in the preceding sections clearly shows the existence of a highly significant excess of strong X-ray sources around the analyzed Seyfert galaxies. Since the Seyfert sample has a high degree of completeness this is a very robust

result. As has been discussed before, the most reliable (i.e. least contaminated) annulus within the extent of the analyzed PSPC field of view is the angular separation from the galaxies between 10 and 25 arcmin. Since we are far off here from the bodies of most of the Seyferts themselves, all excess sources found within this area are not part of the target galaxies but separate objects of mostly extragalactic origin. There are more than 46 strong excess sources associated with the Seyfert galaxies whose X-ray luminosities are typically between one and two orders of magnitude higher than the most luminous X-ray sources of our galaxy. In practice the usual identification of such high latitude X-ray sources turns out to be quasars. To determine their nature and redshift distribution remains the task of a follow-up study which requires extensive work in optical spectroscopy to find out their redshifts. A companion paper gives optical identifications of many of these sources (Arp 1996).

Some of the $C > 10$ sources closer than $10'$ to the Seyfert galaxies may actually coincide with the body of the target galaxy, especially with the closest and brightest Seyferts within the sample. Given their high X-ray luminosity it seems difficult, however, to identify most of these sources with the brightest objects known from our galactic environment, i.e. X-ray binaries and SNR's. That in turn would suggest that also in these cases the sources are active galaxies, QSO's, or other types of extragalactic high-intensity X-ray emitting objects.

The average redshift of the 26 Seyfert galaxies is $z = 0.005$. Assuming that the excess sources found here are at the same redshift distance as the target galaxies this implies a separation of the sources from the galaxies of roughly 100 to 200 kpc ($H_o = 50\ km/s/Mpc$) within the most significant off-axis interval of $10'$ to $20'$. There is thus good agreement with the distance range for which Laurikainen and Salo (1995) find their most significant excess of companions to Seyfert galaxies on the basis of their study of the Palomar Sky Survey.

There is a noticeable tendency in the excess sources discovered in the present analysis of being paired across the Seyferts. There are several cases comparable to an already published example of such a constellation: Analyzing ROSAT PSPC data of NGC 4258 Pietsch et al. (1994) found two strong X-ray sources paired across the nucleus of the Seyfert. A subsequent study by Burbidge (1995) revealed these objects as two quasars at redshifts $z \approx 0.4$ and $z \approx 0.65$, respectively. This example gives further motivation to measure the redshifts of the X-ray objects associated with the other Seyfert galaxies in the present sample.

As a suggestion for an extension of the work presented here I should mention the inclusion of other classes of active galaxies (starbursts, QSOs etc.) in a similar analysis to find out whether the existence of excess X-ray sources is a phenomenon restricted to the Seyfert type or whether it is a feature common to all active galaxies. Additionally, a study of the low-surface brightness X-ray features around the Seyferts using special filtering techniques could give valuable clues to the physical processes going on in the environments of this class of active galaxies as well as to the nature of the objects associated with them.

Acknowledgements. The author owes thanks to Dr. Karen Brazier and Dr. Wolfgang Pietsch for valuable discussions which led to a significant improvement of this paper.

References

Arp, H.C. 1996, A&A in press
Barnes, J.E., Hernquist, L. 1992, ARA&A, 30, 705
Briel, U.G., Pfeffermann, E., Hartner, G. , Hasinger, G. 1988, SPIE, 982, 401
Burbidge, E.M. 1995, A&A, 298, L1
Bushouse, H.A. 1986, AJ, 91, 255
Cruddace, R.G., Hasinger, G., and Schmitt, J. 1988, ESO Conf. Proc. 28, 177
Dahari, O. 1985, ApJS, 57, 643
Dickey, J.M., Lockman, F.J. 1990, ARA&A, 28, 215
Fabbiano, G. 1988, ApJ, 325, 544
Fuentes-Williams, T., Stocke, J.T. 1988, AJ, 96, 1235
Hasinger, G., Turner, J.T., George, I.M., Boese, G. 1992, GSFC OGIP Calibration Memo CAL/ROS/92-001
Hasinger, G., Burg, R., Giacconi, R., et al. 1993, A&A, 275, 1
Laurikainen, E., Salo, H. 1995, A&A, 293, 683
Marston, A.P., Elmegreen, D., Elmegreen, B., et al. 1995, ApJ, 438, 663
McKenty, J.W. 1989, ApJ, 343, 125
McKenty, J.W. 1990, ApJS, 72, 231
Mundell, C.G., Pedlar, A., Axon, D.J., et al. 1995, MNRAS, 277, 641
Petrosian, A.R. 1982, Afz, 18, 548
Pietsch, W., Vogler, A., Kahabka, P., et al. 1994, A&A, 284, 386
Rafanelli, P., Violato, M., Baruffolo, A. 1995, AJ, 109, 1546
Rubin, V.C., Ford, W.K. 1968, ApJ, 154, 431
Sandage, A., Tammann, G. 1981, Revised Shapley-Ames Catalog of Bright Galaxies, Carnegie Institution of Washington
Seyfert, C.K. 1943, ApJ, 97, 28
Turner, T.J., Urry, C.M., Mushotzky, R.F. 1993, ApJ, 418, 653
Vikhlinin, A., Forman, W., Jones, C. et al. 1995, ApJ, 451, 553
Voges, W. 1992, in: Proc. ESA ISY Conference, ESA ISY-3, p.9

This article was processed by the author using Springer-Verlag TEX A&A macro package version 4.

APPENDIX A. Detected Sources with counts rate above 5.0*10^-3 cts/s

Field	RAS(2000) hh mm ss	DEC(2000) dd mm ss	Offaxis Pos. arcmin	Counts Rate 10^-3 cts/s
NGC 1068				
1)	02 42 00.29	00 34 39.5	36.7	6.7
2)	02 41 45.06	00 26 40.0	30.6	8.4
3)	02 42 40.66	00 22 21.0	23.0	9.0
4)	02 40 54.59	00 11 01.5	29.0	6.9
5)	02 43 21.90	00 10 35.0	15.2	5.1
6)	02 41 57.36	00 09 53.0	15.1	5.6
7)	02 42 01.12	00 00 27.0	10.0	6.5
8)	02 44 01.20	00 00 54.5	20.2	5.0
9)	02 39 22.32	-00 01 13.4	49.6	84.5
10)	02 43 25.34	-00 04 12.0	11.7	9.1
11)	02 42 44.40	-00 06 26.5	5.9	15.7
12)	02 45 34.67	-00 07 10.9	44.0	24.2
13)	02 41 34.96	-00 09 24.9	18.7	5.9
14)	02 41 16.12	-00 18 16.9	27.6	9.7
15)	02 43 40.10	-00 25 47.4	29.2	17.8
16)	02 41 13.49	-00 41 24.9	46.3	248.1
NGC 1097				
1)	02 43 42.70	-29 56 38.1	37.7	5.3
2)	02 54 29.99	-30 00 49.9	16.3	6.5
3)	02 47 34.91	-30 02 29.1	19.6	15.9
4)	02 46 03.09	-30 03 17.9	10.5	6.2
5)	02 45 47.94	-30 05 02.2	10.6	5.0
6)	02 45 01.22	-30 07 26.5	17.8	7.4
7)	02 46 50.15	-30 07 45.2	8.6	24.3
8)	02 47 43.02	-30 14 57.3	18.2	6.0
9)	02 46 25.15	-30 17 19.5	4.3	5.0
10)	02 43 37.22	-30 30 44.3	39.1	13.3
11)	02 48 24.02	-30 37 58.3	36.6	15.1
12)	02 47 50.56	-30 38 36.0	32.1	5.5
13)	02 46 25.14	-30 40 26.5	27.3	5.7
14)	02 45 48.33	-30 48 42.7	36.1	11.2
NGC 1365				
1)	03 32 53.12	-35 50 36.0	19.8	5.4
2)	03 33 32.95	-36 06 23.5	2.1	5.2
3)	03 33 44.95	-36 09 51.9	2.3	5.7
4)	03 33 12.26	-36 11 30.8	5.7	6.2
5)	03 33 55.41	-36 16 26.6	41.0	35.7
6)	03 33 12.26	-36 19 31.3	12.1	89.3
7)	03 31 54.44	-36 21 03.8	24.1	8.2
8)	03 33 48.17	-36 24 44.9	16.5	9.7
9)	03 32 09.42	-36 34 50.0	31.7	13.3
10)	03 34 41.73	-36 37 05.3	31.6	13.5
NGC 1566				
1)	04 23 43.81	-54 31 45.5	40.6	9.7
2)	04 20 36.43	-54 31 41.1	25.3	6.1
3)	04 20 12.90	-54 35 56.9	20.5	13.2
4)	04 18 57.27	-54 41 57.0	17.0	11.7
5)	04 23 36.95	-54 42 27.3	34.2	22.5
6)	04 17 16,86	-54 45 10.1	26.0	13.7
7)	04 20 21.58	-54 54 04.9	3.9	7.5
8)	04 23 16.22	-55 06 34.6	29.9	21.8
9)	04 23 59.16	-55 12 15.9	37.7	11.9
10)	04 16 37.53	-55 24 26.6	40.3	5.7

Appendix A continued.

Field	RAS(2000) hh mm ss	DEC(2000) dd mm ss	Offaxis Pos. arcmin	Counts Rate 10^-3 cts/s
NGC 2639				
1)	08 44 13.87	50 40 30.6	28.5	7.0
2)	08 43 10.62	50 33 51.8	21.7	23.4
3)	08 44 19.00	50 31 35.5	20.1	37.8
4)	08 40 02.94	50 30 03.6	38.5	10.4
5)	08 43 55.23	50 28 47.9	16.4	8.2
6)	08 41 37.01	50 25 16.5	23.1	5.2
7)	08 46 08.35	50 07 15.4	24.6	5.8
8)	08 42 29.98	49 57 51.2	18.4	25.7
9)	08 42 34.49	49 41 32.4	32.7	11.0
NGC 2992				
1)	09 44 59.29	-13 47 55.2	33.6	111.0
2)	09 43 37.80	-14 11 24.9	31.5	10.5
3)	09 42 50.55	-14 14 39.1	41.1	5.1
4)	09 47 58.71	-14 15 12.6	33.1	10.0
5)	09 43 37.63	-14 18 01.4	30.5	9.8
6)	09 45 48.75	-14 21 57.0	2.5	15.8
7)	09 43 14.21	-14 23 34.6	36.3	9.3
8)	09 43 29.64	-14 23 01.1	32.5	5.4
9)	09 43 55.53	-14 24 55.4	26.6	6.9
10)	09 45 40.54	-14 34 07.5	14.3	19.1
NGC 3031 (M81)				
1)	09 55 51.28	69 40 38.4	36.5	815.2
2)	09 50 41.30	69 36 24.1	41.1	8.9
3)	09 55 25.52	69 09 56.5	5.8	12.5
4)	09 55 01.68	69 07 42.3	4.4	5.0
5)	09 55 36.37	69 07 02.5	2.9	5.8
6)	09 55 36.36	69 06 28.0	2.3	5.4
7)	09 55 50.93	69 05 33.4	2.2	7.6
8)	09 55 12.01	69 04 56.9	1.9	5.1
9)	09 55 11.18	69 04 09.9	1.8	11.9
10)	09 57 54.13	69 03 47.8	12.8	148.2
11)	09 55 11.09	69 04 06.9	1.8	8.5
12)	09 55 33.83	69 00 36.5	3.6	68.7
13)	10 02 17.25	68 58 40.4	36.8	12.9
14)	09 48 17.63	68 45 18.8	43.3	5.5
15)	09 57 38.64	68 31 59.0	34.2	5.3
NGC 3227				
1)	10 22 44.80	20 28 49.6	38.8	8.3
2)	10 22 58.34	20 22 32.3	31.9	31.9
3)	10 22 13.46	20 19 48.4	33.6	10.2
4)	10 25 52.69	20 03 01.0	35.2	6.5
5)	10 21 48.66	19 59 02.1	25.2	5.5
6)	10 20 55.74	19 54 31.3	36.6	9.1
7)	10 23 26.66	19 53 49.5	2.5	15.0
8)	10 19 42.59	19 52 03.4	53.7	551.4
9)	10 25 12.35	19 50 24.2	23.8	8.7
10)	10 21 54.16	19 47 35.3	23.2	19.7
11)	10 25 52.77	19 47 17.5	33.6	11.0
12)	10 23 37.05	19 36 23.0	15.3	9.0
13)	10 23 38.54	19 32 08.9	19.5	7.0
14)	10 26 50.98	19 30 43.0	51.5	19.2
15)	10 22 38.73	19 27 47.0	26.8	7.1
16)	10 24 42.93	19 12 14.1	42.8	45.6
17)	10 24 00.32	19 06 46.8	45.3	10.4

Appendix A continued.

Field	RAS(2000) hh mm ss	DEC(2000) dd mm ss	Offaxis Pos. arcmin	Counts Rate 10^-3 cts/s
NGC 3516				
1)	11 08 30.89	73 03 36.9	30.4	5.9
2)	11 05 19.46	73 01 33.3	28.1	6.8
3)	11 00 03.13	72 59 30.0	39.2	7.4
4)	11 12 56.38	72 52 39.2	33.0	5.1
5)	11 02 38.90	72 46 41.4	22.4	155.7
6)	11 06 17.73	72 44 13.3	10.3	6.6
7)	11 08 35.52	72 26 11.2	11.4	6.6
8)	11 01 50.77	72 25 50.1	23.9	27.2
9)	11 08 48.06	72 02 41.7	32.8	6.2
10)	11 09 23.92	71 44 00.0	51.6	9.9
NGC 3998				
1)	12 00 09.37	56 13 04.0	49.5	51.4
2)	11 59 37.51	56 02 45.9	38.3	115.6
3)	11 55 18.87	56 01 06.8	40.5	8.7
4)	11 56 34.09	55 59 02.8	33.8	8.9
5)	11 56 32.47	55 47 36.7	23.6	5.1
6)	11 59 36.97	55 46 15.9	23.8	6.1
7)	12 02 34.23	55 41 18.4	41.8	15.8
8)	11 59 51.39	55 32 01.1	17.0	46.2
9)	11 57 53.78	55 27 39.5	0.5	8.1
10)	12 00 42.72	55 03 15.3	33.7	6.7
11)	11 56 54.42	55 02 12.5	26.5	5.9
12)	11 59 05.80	54 48 09.7	40.3	11.2
NGC 4051				
1)	12 02 32.67	45 03 55.6	31.7	5.1
2)	12 06 20.36	44 55 13.4	40.2	7.8
3)	12 03 53.30	44 51 37.5	20.0	30.7
4)	12 05 42.05	44 48 58.9	31.1	14.9
5)	12 02 09.66	44 44 28.4	16.0	72.4
6)	12 05 19.95	44 39 32.0	23.7	17.6
7)	12 00 53.04	44 38 14.2	25.3	5.7
8)	12 03 59.59	44 37 20.4	9.5	8.5
9)	12 04 12.75	44 31 48.5	10.9	16.0
10)	12 03 44.96	44 05 20.2	35.6	6.9
11)	12 05 42.76	44 04 44.7	39.1	6.4
12)	12 02 18.50	44 03 54.7	30.6	17.0
NGC 4151				
1)	12 11 52.85	39 57 18.7	36.3	133.9
2)	12 10 14.55	39 56 40.4	32.2	16.0
3)	12 10 47.82	39 53 18.4	28.9	12.3
4)	12 09 07.88	39 53 21.1	32.9	16.2
5)	12 13 18.55	39 46 32.0	39.0	15.6
6)	12 12 31.96	39 41 35.1	28.8	11.2
7)	12 06 41.29	39 41 02.9	47.2	12.6
8)	12 07 58.83	39 39 42.3	33.0	11.6
9)	12 10 10.64	39 39 33.4	15.5	5.4
10)	12 13 00.65	39 35 58.5	31.0	5.9
11)	12 10 05.08	39 34 39.8	11.2	5.6
12)	12 11 13.68	39 33 24.0	12.1	5.5
13)	12 10 26.58	39 29 04.0	4.5	257.2
14)	12 10 07.57	39 23 11.3	4.7	5.9
15)	12 10 17.20	39 18 21.9	6.8	5.8
16)	12 11 23.30	39 14 18.2	14.4	7.8

Appendix A continued.

Field	RAS(2000) hh mm ss	DEC(2000) dd mm ss	Offaxis Pos. arcmin	Counts Rate 10^-3 cts/s
17)	12 11 10.50	39 12 15.0	14.5	5.1
18)	12 11 14.88	39 11 35.9	15.5	35.1
19)	12 11 16.34	39 11 05.4	16.1	9.2
20)	12 10 32.90	39 09 31.5	15.1	9.1
21)	12 10 43.26	39 07 58.9	16.8	14.3
22)	12 11 09.42	39 07 27.1	18.7	28.5
23)	12 07 59.23	39 07 15.3	34.1	10.0
24)	12 10 27.20	39 07 46.5	16.8	10.3
25)	12 11 28.21	39 04 56.1	22.6	5.6
26)	12 11 34.76	39 00 51.9	26.8	29.1
27)	12 07 19.84	38 52 57.1	48.7	20.2
NGC 4235				
1)	12 15 11.17	07 32 02.5	35.9	267.6
2)	12 16 33.59	07 27 32.9	18.5	10.8
3)	12 16 40.66	07 12 13.9	7.2	14.6
4)	12 19 11.14	07 06 43.5	30.5	5.1
5)	12 15 53.00	06 54 22.1	25.5	6.0
6)	12 16 22.79	06 50 11.3	24.2	15.9
7)	12 19 19.81	06 38 29.3	46.1	119.4
8)	12 17 27.63	06 36 04.4	35.6	8.0
NGC 4258				
1)	12 21 08.82	47 42 07.5	31.8	23.8
2)	12 17 45.15	47 29 15.5	16.3	26.8
3)	12 17 46.68	47 29 13.5	16.1	24.0
4)	12 17 37.71	47 28 57.1	17.1	6.1
5)	12 19 52.20	47 20 57.2	9.1	5.6
6)	12 18 40.75	47 19 04.9	3.2	5.1
7)	12 18 55.06	47 16 31.0	2.5	13.2
8)	12 18 08.35	47 16 13.3	9.1	9.9
9)	12 18 56.88	47 16 01.5	2.9	9.9
10)	12 19 23.14	47 09 36.3	10.1	8.8
NGC 4395				
1)	12 26 31.93	33 47 04.0	16.8	18.3
2)	12 25 57.59	33 46 39.4	13.8	17.3
3)	12 23 33.19	33 45 41.4	30.8	6.5
4)	12 26 56.22	33 43 19.3	17.6	16.0
5)	12 27 49.85	33 38 28.7	26.0	15.9
6)	12 25 58.69	33 33 11.9	2.2	6.6
7)	12 26 57.64	33 32 40.7	14.5	22.0
8)	12 26 01.05	33 31 23.4	3.2	26.0
9)	12 25 31.97	33 25 25.9	8.3	8.1
10)	12 24 40.71	33 24 16.3	16.5	5.3
11)	12 27 35.35	33 09 14.1	32.7	8.7
12)	12 26 23.00	32 44 41.7	48.9	74.0
NGC 4579				
1)	12 37 02.06	12 01 00.8	15.5	8.5
2)	12 39 21.38	11 58 11.9	25.7	7.3
3)	12 38 24.10	11 18 08.8	32.6	14.6
4)	12 37 07.81	11 18 02.3	32.3	6.2
NGC 4594				
1)	12 39 28.43	-11 10 28.8	27.8	7.7
2)	12 38 33.59	-11 23 44.7	25.1	16.2
3)	12 38 26.78	-11 31 49.5	23.4	53.1
4)	12 39 58.80	-11 35 53.5	1.3	8.5
5)	12 39 54.48	-11 36 08.0	1.7	5.9
6)	12 39 50.77	-11 38 00.9	2.4	8.6
7)	12 39 51.69	-11 38 05.4	2.2	15.1

Appendix A continued.

Field	RAS(2000) hh mm ss	DEC(2000) dd mm ss	Offaxis Pos. arcmin	Counts Rate 10^-3 cts/s
8)	12 39 55.74	-11 38 41.5	1.8	6.3
9)	12 39 44.71	-11 38 58.4	4.1	10.2
10)	12 40 03.58	-11 39 46.0	2.7	26.6
11)	12 40 24.60	-11 47 36.4	12.0	5.9
12)	12 38 07.24	-11 59 37.1	35.5	43.8
13)	12 40 58.83	-12 00 13.1	27.2	12.9
14)	12 39 02.02	-12 01 33.6	28.2	5.5
15)	12 40 31.44	-12 04 44.8	28.6	81.7
16)	12 39 53.11	-12 10 26.0	33.3	16.2
NGC 4639				
1)	12 41 31.57	13 39 19.2	30.9	7.5
NGC 4945				
1)	13 05 44.98	-48 55 04.9	33.3	7.0
2)	13 00 58.99	-49 12 17.1	46.4	133.6
3)	13 05 37.44	-49 25 56.4	2.9	8.4
4)	13 08 14.58	-49 26 41.3	27.4	5.2
5)	13 05 20.74	-49 29 30.0	1.6	7.9
6)	13 05 17.50	-49 29 24.5	1.9	13.1
7)	13 05 12.99	-49 30 04.9	2.9	9.0
8)	13 05 11.03	-49 31 08.4	3.8	9.6
9)	13 03 03.42	-49 32 35.0	23.6	10.8
10)	13 09 40.56	-49 32 02.1	41.5	7.7
11)	13 06 34.33	-49 41 19.7	17.1	17.6
12)	13 02 54.13	-49 43 19.3	28.9	15.2
13)	13 06 55.91	-49 54 35.3	30.1	24.1
14)	13 04 58.44	-49 59 16.3	31.4	5.5
15)	13 05 16.11	-50 15 48.9	47.6	10.2
NGC 5005				
1)	13 11 12.37	37 38 05.9	34.6	27.8
2)	13 11 18.96	37 24 59.8	21.8	10.0
3)	13 12 33.25	37 23 37.1	27.6	13.4
4)	13 12 18.73	37 11 25.2	18.0	9.1
5)	13 10 56.57	37 03 03.5	0.6	7.0
6)	13 12 53.09	37 02 03.0	23.1	7.7
7)	13 13 49.36	36 53 46.2	35.7	18.3
8)	13 13 26.51	36 35 27.1	41.0	152.2
9)	13 13 24.77	36 32 58.2	42.5	26.6
10)	13 11 54.70	36 27 38.6	37.7	6.2
NGC 5033				
1)	13 10 58.06	37 03 05.3	40.6	25.5
2)	13 12 52.89	37 01 34.7	27.0	10.9
3)	13 14 03.58	36 54 30.1	20.5	9.5
4)	13 13 48.78	36 53 47.8	18.9	21.1
5)	13 15 28.37	36 35 33.6	24.5	5.0
6)	13 15 50.02	36 24 14.1	31.0	39.7
7)	13 15 28.37	36 22 46.1	27.6	9.1
8)	13 12 32.86	36 13 26.2	24.5	5.7
9)	13 14 12.11	36 10 58.4	26.1	6.7
10)	13 15 39.89	36 10 29.3	36.7	17.1
11)	13 10 37.08	35 56 30.9	51.7	301.9
NGC 5128 (Cen A)				
1)	13 25 15.33	-42 33 37.9	27.7	7.1
2)	13 27 26.13	-42 40 16.7	30.0	28.5
3)	13 28 33.06	-42 41 23.2	39.2	15.6
4)	13 26 57.79	-42 41 53.8	25.3	5.3
5)	13 26 04.95	-42 46 55.6	15.7	6.9

Appendix A continued.

Field	RAS(2000) hh mm ss	DEC(2000) dd mm ss	Offaxis Pos. arcmin	Counts Rate 10^-3 cts/s
6)	13 24 33.59	-42 56 03.1	11.3	8.3
7)	13 25 23.17	-42 57 05.5	4.2	8.2
8)	13 25 38.02	-43 02 28.9	2.1	5.4
9)	13 25 04.97	-43 02 17.3	4.5	8.1
10)	13 25 14.95	-43 02 44.9	37.7	9.5
11)	13 25 13.18	-43 02 10.4	3.0	13.5
12)	13 26 25.95	-43 02 43.6	10.6	5.3
13)	13 25 27.82	-43 03 23.0	2.2	9.5
14)	13 25 08.06	-43 04 00.4	4.7	29.5
15)	13 25 58.87	-43 04 17.7	6.3	5.7
16)	13 25 18.87	-43 04 40.4	3.9	6.2
17)	13 26 01.76	-43 05 18.7	7.3	7.9
18)	13 25 44.39	-43 10 41.4	9.9	11.8
19)	13 23 06.28	-43 20 30.0	32.4	10.8
20)	13 23 56.33	-43 20 32.2	25.6	5.2
NGC 5273				
1)	13 40 01.17	36 10 20.9	40.4	7.2
2)	13 43 00.80	36 09 51.7	32.7	46.6
3)	13 40 01.00	36 10 18.4	40.4	7.6
4)	13 42 16.29	36 06 21.4	27.4	23.2
5)	13 41 14.44	35 53 38.2	18.1	7.8
6)	13 44 17.38	35 45 21.1	27.2	39.2
7)	13 40 54.06	35 40 53.1	15.0	6.7
8)	13 39 42.65	35 39 35.6	29.4	6.9
9)	13 41 33.14	35 32 57.7	9.2	18.2
10)	13 39 58.06	35 23 25.6	30.5	9.2
11)	13 42 55.73	35 21 39.4	20.0	12.6
12)	13 42 27.14	35 07 10.9	32.1	5.3
NGC 5548				
1)	14 17 29.54	25 53 42.3	45.8	17.1
2)	14 16 58.27	25 44 53.2	39.1	6.1
3)	14 17 57.22	25 43 32.5	35.1	1213.0
4)	14 21 04.09	25 37 51.9	51.0	9.9
5)	14 17 11.36	25 34 33.0	28.4	12.3
6)	14 17 59.70	25 25 05.0	16.7	8.7
7)	14 19 12.89	25 16 32.3	18.4	6.3
8)	14 20 53.58	25 14 17.1	39.7	8.0
9)	14 17 22.88	25 13 44.2	10.0	7.6
10)	14 18 33.43	25 12 38.7	8.7	5.2
11)	14 18 31.66	25 12 38.8	8.3	5.2
12)	14 19 38.12	25 12 04.9	22.5	6.8
13)	14 18 30.66	25 10 59.8	7.4	35.1
14)	14 18 57.50	25 09 52.8	13.1	10.3
15)	14 20 41.55	25 08 35.5	36.6	12.4
16)	14 15 55.90	25 01 59.7	28.8	5.0
17)	14 20 12.13	24 56 17.8	32.2	10.1
18)	14 16 49.94	24 35 24.9	36.6	9.0
19)	14 18 21.34	24 34 36.4	43.1	8.3
20)	14 18 49.62	24 31 22.9	38.7	10.0
NGC 7213				
1)	22 11 36.26	-46 48 35.8	31.8	13.0
2)	22 09 16.83	-47 07 57.0	11.4	6.8
3)	22 07 00.13	-47 12 27.7	23.7	5.4
4)	22 13 14.08	-47 13 29.5	40.0	21.7
5)	22 09 01.15	-47 16 09.4	6.7	5.4

Appendix A continued.

Field		RAS(2000) hh mm ss	DEC(2000) dd mm ss	Offaxis Pos. arcmin	Counts Rate 10^-3 cts/s
NGC 7314					
	1)	22 33 54.89	-25 51 17.8	27.5	12.8
	2)	22 37 34.17	-25 54 23.9	25.9	8.7
	3)	22 35 48.00	-26 01 24.5	1.7	10.2
	4)	22 37 51.37	-26 05 03.6	28.3	10.6
	5)	22 36 06.01	-26 07 53.4	6.7	6.8
	6)	22 37 50.47	-26 11 10.6	29.2	7.1
	7)	22 34 23.19	-26 13 04.0	21.0	7.2
	8)	22 34 56.58	-26 20 48.4	20.9	11.7
	9)	22 37 14.51	-26 22 28.8	27.9	91.3
CONTROL FIELDS					
HR 857					
	1)	02 50 57.56	-12 25 57.9	30.5	11.8
	2)	02 53 02.39	-12 35 30.3	13.1	8.1
	3)	02 52 00.84	-12 44 59.8	7.5	6.1
	4)	02 50 39.84	-12 49 49.5	27.4	5.9
	5)	02 50 41.79	-12 49 56.5	26.9	10.0
	6)	02 54 50.56	-12 58 29.2	36.1	32.8
	7)	02 52 35.31	-13 06 04.0	19.9	33.8
	8)	02 53 46.71	-13 08 17.3	28.7	8.1
	9)	02 52 44.80	-13 13 33.4	27.6	16.9
	10)	02 53 07.42	-13 21 21.8	36.3	9.5
	11)	02 51 07.08	-13 22 55.6	42.1	14.0
	12)	02 51 52.81	-13 25 56.8	40.8	26.1
EF Eri					
	1)	03 14 12.84	-22 36 12.0	39.4	1194.3
	2)	03 12 02.67	-22 46 36.6	41.5	12.1
	3)	03 16 12.15	-22 47 45.1	39.2	10.7
	4)	03 16 22.04	-22 50 44.1	38.9	5.7
	5)	03 11 45.97	-22 54 35.7	39.6	33.2
	6)	03 13 37.79	-23 03 19.7	14.6	12.0
	7)	03 14 43.03	-23 06 38.8	11.4	8.3
	8)	03 14 17.48	-23 09 31.0	6.2	11.3
	9)	03 13 47.56	-23 18 34.3	6.4	7.6
	10)	03 12 14.80	-23 37 14.2	34.5	12.8
VW Hyi					
	1)	04 06 43.96	-71 16 34.3	11.9	19.6
	2)	04 06 56.14	-71 17 12.9	10.9	7.8
	3)	04 06 41.88	-71 17 26.7	12.0	6.2
	4)	04 06 52.78	-71 17 30.3	11.2	7.6
	5)	04 09 16.18	-71 18 05.5	0.8	6.1
	6)	04 14 02.37	-71 24 03.1	24.2	6.9
	7)	04 08 05.61	-71 27 04.3	11.0	25.7
	8)	04 14 23.73	-71 35 24.6	30.7	6.6
	9)	04 06 59.05	-71 40 53.1	25.7	13.7
	10)	04 08 54.40	-72 03 32.4	46.2	8.7
F 1557					
	1)	04 08 15.90	-65 16 30.2	45.0	10.1
	2)	04 07 13.90	-65 28 58.9	41.5	10.1
	3)	04 15 46.05	-65 34 36.0	24.0	5.0
	4)	04 06 07.05	-65 35 42.7	44.7	28.1
	5)	04 08 39.86	-65 45 44.7	26.7	51.1
	6)	04 11 42.43	-65 46 45.9	8.6	5.3
	7)	04 19 16.21	-65 57 50.6	39.5	36.9

Appendix A continued.

Field		RAS(2000) hh mm ss	DEC(2000) dd mm ss	Offaxis Pos. arcmin	Counts Rate 10^-3 cts/s
	8)	04 10 13.25	-66 12 04.2	26.7	12.6
	9)	04 15 28.21	-66 19 34.3	32.5	25.1
	10)	04 16 01.65	-66 28 48.1	42.2	39.8
Uma					
	1)	10 24 35.46	42 02 11.0	41.0	7.6
	2)	10 22 17.12	41 55 31.0	25.5	12.7
	3)	10 25 01.86	41 43 14.3	33.2	9.7
	4)	10 24 23.09	41 41 48.8	26.0	23.0
	5)	10 21 46.70	41 34 34.2	7.6	7.9
	6)	10 20 24.70	41 33 34.9	21.7	17.2
	7)	10 23 28.45	41 29 13.2	13.0	5.1
	8)	10 21 42.12	41 14 32.1	17.0	10.2
	9)	10 23 42.31	41 11 29.6	24.2	14.3
	10)	10 19 55.52	40 59 44.8	40.6	95.8
	11)	10 22 53.64	40 58 05.6	32.6	7.9
	12)	10 22 21.11	40 56 50.0	33.2	8.9
CY Uma					
	1)	10 56 27.66	50 20 00.7	38.9	10.9
	2)	10 59 12.35	50 01 15.6	29.4	5.7
	3)	10 59 34.60	49 43 00.8	25.5	19.9
	4)	10 53 44.62	49 30 24.4	33.1	28.3
	5)	10 59 51.85	49 16 49.7	37.5	6.6
ON 231					
	1)	12 23 54.75	28 29 14.8	34.3	10.5
	2)	12 19 53.80	28 26 23.3	24.9	5.5
	3)	12 19 48.25	28 22 45.6	24.4	12.4
	4)	12 22 15.38	28 21 18.5	12.3	6.6
	5)	12 23 10.23	28 09 21.1	22.3	5.4
	6)	12 21 35.63	28 06 11.5	7.7	9.2
4 Dra					
	1)	12 27 02.97	69 29 15.4	23.7	6.9
	2)	12 30 55.88	69 25 38.1	14.3	5.2
	3)	12 25 37.30	69 22 40.9	26.1	8.0
	4)	12 34 28.43	69 19 45.7	24.4	8.1
	5)	12 33 23.69	69 10 05.5	17.6	25.5
	6)	12 20 48.97	69 05 36.3	50.1	78.9
	7)	12 30 51.67	69 05 17.1	7.8	9.3
	8)	12 35 51.48	69 00 40.3	32.7	70.9
	9)	12 37 32.05	68 59 05.3	41.7	8.0
	10)	12 35 19.87	68 53 21.5	33.6	9.5
	11)	12 32 09.25	68 46 53.2	27.4	6.3
	12)	12 31 28.05	68 38 49.3	34.0	6.5
EX Hya					
	1)	12 54 26.12	-28 29 09.5	53.1	36.6
	2)	12 52 44.70	-28 36 42.4	38.6	33.7
	3)	12 51 59.86	-28 41 21.8	34.0	8.2
	4)	12 52 21.40	-28 51 50.5	23.2	5.0
	5)	12 51 54.53	-28 59 53.8	16.4	5.0
	6)	12 54 20.37	-29 00 17.8	29.4	211.7
	7)	12 54 40.60	-29 13 44.6	29.8	344.2
	8)	12 52 04.72	-29 20 42.9	7.1	8.1
	9)	12 52 14.52	-29 34 57.4	20.1	5.7
	10)	12 48 59.63	-29 34 36.3	48.6	15.3
	11)	12 51 35.74	-29 58 39.4	44.9	78.3

Appendix A continued.

Field		RAS(2000) hh mm ss	DEC(2000) dd mm ss	Offaxis Pos. arcmin	Counts Rate 10^-3 cts/s
Alpha Bootis					
	1)	14 17 15.57	19 39 23.9	35.8	19.2
	2)	14 15 41.52	19 36 53.0	25.5	20.7
	3)	14 15 06.94	19 14 29.3	8.6	12.0
	4)	14 15 40.89	19 06 54.5	4.5	5.2
	5)	14 15 36.11	19 06 10.0	5.3	9.4
LHS 2924					
	1)	14 29 04.04	33 50 18.9	39.8	121.1
	2)	14 27 45.42	33 38 19.6	30.1	6.5
	3)	14 28 12.23	33 20 00.2	11.3	5.7
	4)	14 26 52.69	33 09 33.9	23.2	5.8
	5)	14 30 39.13	33 07 59.6	24.4	6.8
	6)	14 27 38.17	33 53 09.4	22.3	5.4
	7)	14 31 19.38	32 50 50.3	38.3	23.0
	8)	14 27 57.67	32 47 38.9	25.0	29.0
	9)	14 27 50.49	32 43 42.3	29.3	8.1
	10)	14 28 40.98	32 31 53.5	38.9	38.9
Pavo					
	1)	21 15 28.22	-67 35 16.3	15.0	12.8
	2)	21 10 07.02	-67 49 07.4	24.3	5.4
	3)	21 16 35.60	-67 51 14.2	13.0	5.5
	4)	21 20 36.58	-67 51 49.1	35.4	11.5
	5)	21 14 20.39	-68 00 58.5	13.6	15.9
	6)	21 13 35.12	-68 19 41.0	32.6	9.4
GRB 790406					
	1)	23 15 11.30	-49 16 51.1	25.5	10.0
	2)	23 12 45.58	-49 27 25.5	17.1	8.5
	3)	23 13 17.13	-49 33 21.0	9.3	35.7
	4)	23 13 15.02	-49 33 26.9	9.5	5.9
	5)	23 17 38.79	-49 33 37.1	35.9	27.6
	6)	23 16 19.45	-49 39 15.2	22.6	5.8
	7)	23 17 27.75	-49 59 04.9	38.8	14.2
	8)	23 15 44.96	-50 03 44.5	29.5	5.7
HR 8905					
	1)	23 26 42.13	23 44 26.2	27.5	11.8
	2)	23 27 38.04	23 35 05.8	33.2	11.6
	3)	23 23 04.61	23 27 11.2	31.6	15.5
	4)	23 23 15.71	23 21 16.3	29.0	6.3
	5)	23 24 50.23	23 21 08.3	7.8	5.2
	6)	23 27 08.89	23 14 58.7	26.2	9.5
	7)	23 25 48.39	22 54 46.8	29.9	5.1
	8)	23 24 17.67	22 52 10.1	35.1	5.5
	9)	23 22 55.47	22 44 49.2	51.6	27.2